

3D FINITE ELEMENT MODELING OF CURRENT DENSITIES IN SEMICONDUCTOR TRANSPORT WITH IMPACT IONIZATION

A. MAURI¹, A. BORTOLOSSI², G. NOVIELLI³, AND R. SACCO⁴

ABSTRACT. In this article we propose two novel 3D finite element models, denoted method A and B, for electron and hole Drift-Diffusion (DD) current densities. Method A is based on a primal-mixed formulation of the DD model as a function of the quasi-Fermi potential gradient, while method B is a modification of the standard DD formula based on the introduction of an artificial diffusion matrix. Both methods are genuine 3D extensions of the classic 1D Scharfetter-Gummel difference formula. The proposed methods are compared in the 3D simulation of a p - n junction diode and of a p -MOS transistor in the on-state regime. Results show that method A provides the best performance in terms of physical accuracy and numerical stability. Method A is then used in the 3D simulation of a n -MOS transistor in the off-state regime including the impact ionization generation mechanism. Results demonstrate that the model is able to accurately compute the I-V characteristic of the device until drain-to-bulk junction breakdown.

Keywords: Drift-Diffusion model; Finite Element method; Numerical Simulation; Impact Ionization; PACS:85.30; MSC 2000: 35J; 65N30.

1. INTRODUCTION AND MOTIVATION

Semiconductor technology is undergoing a continuously increasing advancement in the aggressive scaling of device length [10]. In this scenario, three-dimensional (3D) device modeling and numerical simulation techniques play a critical role in the prediction of the electrical performance of the system under investigation. The result of our approach to 3D modeling and simulation of semiconductor device applications (see [22] and [20]) is the FEMOS project (Finite Element Modeling Oriented Simulator), a general-purpose modular numerical code based on the use of the Galerkin Finite Element Method (GFEM) implemented in a fully 3D framework through shared libraries using an objected-oriented programming language (C++). In the present work we employ the FEMOS computational platform in the study of the *Drift Diffusion model* (DD) [27, 18] and focus on the issue of endowing the simulation tool of a consistent, stable and accurate procedure for the approximation of electron and hole current densities in the device. This is of utmost importance in: i) visualization and post-processing; ii) evaluation of conduction currents at device terminals; and iii) inclusion in the DD model of generation phenomena due to Impact Ionization (II). Here, our attention is devoted to iii), because of the critical role of II in the convergence and numerical stability of the iterative algorithm used to solve the DD system (see [19], Chapt. 3 and [21]), although the methods we propose for the treatment of iii) can also be profitably employed for i) and ii).

To allow a consistent treatment of the generation term due to II within the FE procedure, we propose two novel discrete models for electron and hole current densities over the computational grid. The two methods provide a constant approximation of

Date: December 12, 2014.

the current density inside each mesh element and for this reason they can be easily implemented in any simulation environment not necessarily employing the GFEM but utilizing, instead, the more standard Box Integration Method (see [4, 5] and [27], Chapt. 6). The first scheme (method A) is based on the use of a primal-mixed formulation of the DD model written as a function of the quasi-Fermi potential gradient (see [24] and [26]). The second scheme (method B) is a modification of the standard DD formula based on the introduction of an artificial diffusion matrix (see also [3]). Both methods are genuine 3D extensions of the classic Scharfetter-Gummel (SG) formula for the computation of the current density over a 1D element [15].

The proposed finite element models are validated in the numerical study of 3D device structures (p - n junction diode and MOS transistors) under on-state and off-state regimes. Results clearly indicate that method A provides the best performance in terms of physical accuracy and numerical stability, and demonstrate the ability of the simulation model in accurately computing the I-V characteristic of the device until the onset of drain-to-bulk junction breakdown.

The outline of the article is as follows. In Sect. 2 we briefly review the DD model and its finite element discretization. In Sect. 3 we illustrate the novel methods proposed to calculate the current densities in the device. In Sect. 4 we carry out their extensive validation by comparing the obtained results with a reference simulation suite in the study of 3D p - n and MOS structures including the II generation term. Concluding remarks and perspectives are addressed in Sect. 5.

2. TRANSPORT MODEL AND DISCRETIZATION

The Drift-Diffusion (DD) equations for electron and hole current densities \mathbf{J}_n and \mathbf{J}_p in a semiconductor device are:

$$(1a) \quad \mathbf{J}_n = q\mu_n n \mathbf{E} + qD_n \nabla n$$

$$(1b) \quad \mathbf{J}_p = q\mu_p p \mathbf{E} - qD_p \nabla p$$

where n and p are the densities of electrons and holes, $\mathbf{E} = -\nabla\varphi$ is the electric field, φ being the electric potential, while μ_n and μ_p are the electron and hole mobilities and D_n and D_p are the electron and hole diffusivities, related to the mobilities through Einstein's relation. We refer to [27, 19, 18] for an extensive analysis and discussion of the DD model. To iteratively solve the differential equation system constituted by the Poisson equation for φ and the continuity equations for n and p we adopt the Gummel decoupled solution map with the lagging technique for the treatment of recombination and generation mechanisms. We refer to [14] and [18] for a description and thorough analysis of the solution map.

The device under investigation is geometrically represented by the polyhedral domain $\Omega \subset \mathbb{R}^3$, given by the union of two open disjoint subsets, a doped silicon part and an oxide part assumed to be a perfect insulator, separated by an interfacial surface. For the numerical simulation of the DD model, the domain Ω is divided in a discrete partition \mathcal{T}_h made by elements K , each element being a tetrahedron of volume $|K|$, such that $\bar{\Omega} = \bigcup_{K \in \mathcal{T}_h} \bar{K}$. Then, each differential problem in the Gummel decoupled algorithm is written in weak form (see [23], Chapt. 5) and discretized using the displacement-based Galerkin Finite Element Method (GFEM) with piecewise linear conforming elements for potential and carrier densities (see [23], Chapt. 6). To avoid numerical instabilities due to possible dominance of the drift term, the variant of the GFEM denoted Edge Averaged Finite Element (EAFE)

method proposed and analyzed in [28, 29] is used in the solution of the linearized continuity equations for electrons and holes.

3. FINITE ELEMENT MODELS FOR THE CURRENT DENSITY

The construction of a stable and accurate approximate current density field in a primal-based FE formulation is not a trivial task because of possible numerical problems arising from differentiation and cancellation in the DD transport relations (1a)-(1b). In this section we introduce two novel finite element methodologies for current density discretization. The proposed approaches have a cheap computational cost compared to other formulations (such as the dual-mixed FEM, see [7]), are completely compatible for use in the classical Box Integration Method (BIM [4, 5]) and are genuine 3D extensions of the classic Scharfetter-Gummel (SG) 1D difference formula [15]. In the remainder of the article, for a given element K in \mathcal{T}_h we denote the volume of K by $\text{vol}(K)$; moreover, with the subscript K we refer to a quantity defined in the interior of K while the subscript h refers to a quantity defined at the vertices of K . For a given function $f : K \rightarrow \mathbb{R}$ we define $\langle f \rangle_K := \int_K f dK / \text{vol}(K)$ the mean integral value of f over K . We also assume that carrier mobility (and the associated diffusivity through Einstein's relation) is constant in K , while the electric potential is linear (so that the associated electric field is a constant vector in K).

3.1. The DD Formula. The simplest FE model for the current densities (method DDFE) is obtained by replacing into the transport equations (1a)-(1b) the functions n , p and φ with their corresponding FE approximations n_h , p_h and φ_h , and then by computing the integral average of the resulting expressions over the element K . This yields

$$(2a) \quad \mathbf{J}_{n,K} = q\mu_n \langle n \rangle_K \mathbf{E}_K + qD_n \nabla n_{h,K}$$

$$(2b) \quad \mathbf{J}_{p,K} = q\mu_p \langle p \rangle_K \mathbf{E}_K - qD_p \nabla p_{h,K}.$$

It is immediate to see that the discrete current densities (2a) and (2b) automatically reproduce the limiting cases of pure diffusive flow ($\mathbf{E}_K = \mathbf{0}$) and pure ohmic flow ($n_{h,K} = \text{constant}$ and $p_{h,K} = \text{constant}$). In the case of thermal equilibrium ($\mathbf{J}_{n,K} = \mathbf{J}_{p,K} = \mathbf{0}$), we can anticipate computational difficulties with the use of (2a) and (2b) because of exact cancellation of drift and diffusive current contributions. Thus, by a continuity argument, we also see that method DDFE does not seem appropriate in the numerical treatment of the subthreshold current regime, where currents are not exactly equal to zero but are very small. The two following formulations are designed to overcome this limitation.

3.2. Method A. To describe method A we consider the case of electron continuity equation because a completely similar treatment holds for the hole continuity equation. We start from the Maxwell-Boltzmann (MB) statistics for electrons $n = n_i \exp((\varphi_n - \varphi)/V_{th})$ where n_i is the intrinsic concentration in the semiconductor material, φ_n is the quasi-Fermi potential for electrons and V_{th} is the thermal voltage. Replacing the MB relation into (1a) yields the equivalent (nonlinear) gradient form of the electron current density

$$(3a) \quad \mathbf{J}_n = -q\mu_n n \nabla \varphi_n = -q\mu_n n_i \exp((\varphi_n - \varphi)/V_{th}) \nabla \varphi_n.$$

To construct the finite element model for \mathbf{J}_n as in (3a), we use the primal-mixed (PM) FEM introduced and analyzed in [24] and recently extended to the case of

advective-diffusive operators in [26]. In the PM FEM of lowest order, the approximate current density is constant over each $K \in \mathcal{T}_h$ while the approximate quasi-Fermi potential is piecewise linear and continuous over \mathcal{T}_h . Let us introduce the finite element spaces of piecewise constant and piecewise linear continuous functions over \mathcal{T}_h :

$$(3b) \quad Q_h = \{w \in L^2(\Omega) : w|_K \in \mathbb{P}_0(K) \forall K \in \mathcal{T}_h\}$$

$$(3c) \quad V_h = \{u \in C^0(\bar{\Omega}) : u|_K \in \mathbb{P}_1(K) \forall K \in \mathcal{T}_h\}$$

and the electrical conductivity $\sigma_{n,h} := q\mu_n n_i \exp((\varphi_n - \varphi)/V_{th})$. Then, the PM-FE approximation of (3a) reads: find $\mathbf{J}_{n,h} \in [Q_h]^3$ such that

$$(3d) \quad \int_{\Omega} \sigma_{n,h}^{-1} \mathbf{J}_{n,h} \cdot \mathbf{q}_h \, d\Omega + \int_{\Omega} \nabla \varphi_{n,h} \cdot \mathbf{q}_h \, d\Omega = 0 \quad \forall \mathbf{q}_h \in [Q_h]^3$$

where $\mathbf{J}_{n,h} \in [Q_h]^3$, $\varphi_{n,h} \in V_h$ and $\varphi_h \in V_h$ are the finite element discrete analogues of \mathbf{J}_n , φ_n and φ . Since functions in $[Q_h]^3$ are discontinuous, relation (3d) amounts to

$$(3e) \quad \int_K \sigma_{n,h}^{-1} \mathbf{J}_{n,h} \cdot \mathbf{q}_h \, dK + \int_K \nabla \varphi_{n,h} \cdot \mathbf{q}_h \, dK = 0 \quad \forall \mathbf{q}_h \in [\mathbb{P}_0(K)]^3.$$

Using in (3e) the standard basis functions for $[\mathbb{P}_0(K)]^3$ we obtain

$$(3f) \quad [\mathbf{J}_{n,h}]_i = -\mathcal{H}_K(\sigma_{n,h}) \frac{\partial \varphi_{n,h}}{\partial x_i} \quad i = 1, 2, 3, \quad \forall K \in \mathcal{T}_h$$

where $\mathcal{H}_K(\sigma_{n,h}) := (\langle \sigma_{n,h}^{-1} \rangle_K)^{-1}$ is the harmonic average of $\sigma_{n,h}$ over the element K .

To numerically compute in a simple and accurate manner the harmonic average of the electrical conductivity, we use the following quadrature rule (see also [6, 8])

$$(3g) \quad \left(\frac{\int_K \sigma_{n,h}^{-1} \, dK}{\text{vol}(K)} \right)^{-1} \simeq \left(\frac{\int_{e^*} \sigma_{n,h}^{-1} \, de}{|e^*|} \right)^{-1}$$

e^* being the edge of ∂K where the maximum drop of $\sigma_{n,h}$ occurs and $|e^*|$ its euclidean length. To identify the edge e^* we introduce the linear dimensionless potential $\Phi := (\varphi_h - \varphi_{n,h})/V_{th}$ and we determine the two vertices: \mathbf{x}_m s.t. $\Phi(\mathbf{x}_m) = \Phi_m := \min_K(\Phi)$ and \mathbf{x}_M s.t. $\Phi(\mathbf{x}_M) = \Phi_M := \max_K(\Phi)$. Then, we define e^* to be the edge of ∂K which connects \mathbf{x}_m and \mathbf{x}_M . The evaluation of the approximate 1D integral in (3g) by choosing the orientation from \mathbf{x}_m and \mathbf{x}_M yields

$$(3h) \quad \int_K \sigma_{n,h}^{-1} \, dK \simeq q\mu_n n_i \exp(\Phi_m) \mathcal{B}(\Phi_m - \Phi_M)$$

while choosing the orientation from \mathbf{x}_M and \mathbf{x}_m the result is

$$(3i) \quad \int_K \sigma_{n,h}^{-1} \, dK \simeq q\mu_n n_i \exp(\Phi_M) \mathcal{B}(\Phi_M - \Phi_m),$$

where $\mathcal{B}(Z) := Z/(\exp(Z) - 1)$ is the inverse of the Bernoulli function, such that $\mathcal{B}(0) = 1$. Using MB statistics into the previous two relations, the property $e^Z \mathcal{B}(Z) = \mathcal{B}(-Z)$, and combining (3h) and (3i), we find

$$(3j) \quad \mathbf{J}_{n,K} = -q\mu_n \left[\frac{n_m \mathcal{B}(-\Delta \Phi_{max}) + n_M \mathcal{B}(\Delta \Phi_{max})}{2} \right] \nabla \varphi_{n,h}$$

where $n_m := n_i e^{\Phi_m}$ and $n_M := n_i e^{\Phi_M}$ while $\Delta \Phi_{max} := \Phi_M - \Phi_m$.

Remark 3.1 (Method A and the 1D SG scheme). *The approximate electron current density (3j) can be regarded as a consistent extension to the 3D case of the classic 1D SG formula, provided to replace over the tetrahedron K the 1D gradient of the electron quasi Fermi potential φ_n with the constant 3D gradient of the approximation $\varphi_{n,h}|_K$, and the electrical conductivity σ_n with the constant electrical conductivity $\sigma_{n,h}|_K$ defined (as in the SG formula) as the 1D harmonic average of σ_n over the interval $[\mathbf{x}_m, \mathbf{x}_M]$.*

Following the same procedure also for the hole current density we have

$$(3k) \quad \mathbf{J}_{p,K} = -q\mu_p \left[\frac{p_m \mathcal{B}(\Delta\Phi_{max}) + p_M \mathcal{B}(-\Delta\Phi_{max})}{2} \right] \nabla \varphi_{p,h}.$$

3.3. Method B. In the previous section the discrete form of the current density is constructed by starting from the equivalent "ohmic" representation in terms of the quasi Fermi potential, and then by performing a suitable approximation of the electrical conductivity over the finite element K . Here, we continue along the same line of thought, but starting from the classic DD format (1a)- (1b), with the intent of using the method of Streamline Upwind artificial diffusion proposed in [9] for the advective-diffusive model to stabilize the computation in the presence of a high electric field.

3.3.1. The 1D SG Method as an Artificial Diffusion Scheme. In the 1D setting the artificial diffusion technique consists of replacing the electron diffusion coefficient D_n with the modified quantity

$$(4a) \quad D_{n,h} = D_n + D_n \Phi(\mathbb{P}e|_K)$$

where Φ is a suitable nonnegative stabilization function of the 1D local Péclet number $\mathbb{P}e|_K = (h|\partial_x \varphi_h|)/(2V_{th}) = |\Delta\varphi|/(2V_{th})$, h and $\Delta\varphi$ being the length of the 1D interval and the potential drop over the interval, respectively. The local Péclet number gives a measure of how much the drift term dominates over the diffusion term in the transport mechanism. If $\mathbb{P}e|_K > 1$ the problem is locally drift (advection)-dominated and in such a case we need introduce an extra amount of diffusion in (4a) (given by $D_n \Phi(\mathbb{P}e|_K)$) to prevent the occurrence of unphysical spurious oscillations in the computed solution, which might even lead to a negative electron concentration. If $\mathbb{P}e|_K < 1$ the problem is locally diffusion-dominated and there is no need of adding an extra diffusion, so that the standard GFEM is enough for obtaining an accurate and numerically stable solution. Based on the last observation, the function Φ has to satisfy the property of consistency

$$(4b) \quad \lim_{\mathbb{P}e|_K \rightarrow 0} \Phi(\mathbb{P}e|_K) = 0 \quad \forall K \in \mathcal{T}_h.$$

The 1D approximation of the electron current density to be used in a stabilized GFEM is thus given by the following relation

$$(4c) \quad J_{n,h}(n_h)|_K = q\mu_n \langle n \rangle_K E_{h,K} + qD_n (1 + \Phi(\mathbb{P}e|_K)) \partial_x n_h \quad \forall K \in \mathcal{T}_h.$$

To design in a physically sound and consistent manner the optimal stabilization function Φ , we pretend the modified method to exactly satisfy some limiting cases that often occur in practical important electronic applications. Using a 3D notation, for sake of generality and because this will be used in later extension, the considered cases are:

- C1. **Constant carrier concentrations** (only drift contribution): $\mathbf{J}_n = q\mu_n n \mathbf{E}$.
 C2. **Constant potential** ($\mathbf{E} = 0$, only diffusive contribution): $\mathbf{J}_n = qD_n \nabla n$.
 C3. **Constant quasi Fermi potential** (no current flow): $\mathbf{J}_n = -q\mu_n n \nabla \varphi_n = \mathbf{0}$.

Notice that case C3. implies that

$$(4d) \quad n = C e^{\varphi/V_{th}}$$

where C is an arbitrary constant such that $C = \exp(-\bar{\varphi}_n/V_{th})$, $\bar{\varphi}_n$ being a given constant value. Thanks to assumption (4b) the stabilized current (4c) automatically satisfies cases C1 and C2. Case C3 is recovered by imposing (in the 1D setting)

$$(4e) \quad J_{n,h}(\Pi_1^K(C e^{\varphi/V_{th}})) = 0$$

where Π_1^K is the \mathbb{P}_1 -interpolant over the element K . Using (4e) in (4c), noting that $E_K = -\partial_x \varphi_h$ and using Einstein's relation, we obtain the following relation for the stabilization function

$$(4f) \quad \Phi(\mathbb{P}e|_K) = \frac{\langle n \rangle_K}{V_{th}} \frac{\partial_x \varphi_h}{\partial_x \Pi_1^K(e^{\varphi/V_{th}})} - 1.$$

Enforcing relation (4d) at the two vertices x_i of the interval, $i = 1, 2$, yields

$$(4g) \quad \Phi(\mathbb{P}e|_K) = \sigma \mathbb{P}e|_K \frac{e^{\varphi_1/V_{th}} + e^{\varphi_2/V_{th}}}{e^{\varphi_2/V_{th}} - e^{\varphi_1/V_{th}}} - 1 = \sigma \mathbb{P}e|_K \frac{e^{2\sigma \mathbb{P}e|_K} + 1}{e^{2\sigma \mathbb{P}e|_K} - 1} - 1$$

where n_1 and n_2 are the two nodal values of n_h while $\sigma := \text{sign}(\Delta\varphi)$. Setting for brevity $X := 2\sigma \mathbb{P}e|_K$, relation (4g) becomes

$$\begin{aligned} \Phi(X) &= \frac{X}{2} \left(\frac{e^X}{e^X - 1} + \frac{1}{e^X - 1} \right) - 1 = \frac{1}{2} (\mathcal{B}(-X) + \mathcal{B}(X)) - 1 \\ &= \frac{1}{2} (X + \mathcal{B}(X) + \mathcal{B}(X)) - 1 = \mathcal{B}(X) + \frac{X}{2} - 1, \end{aligned}$$

and replacing the definition of X we obtain for both $\Delta\varphi > 0$ and $\Delta\varphi < 0$

$$(4h) \quad \Phi(\mathbb{P}e|_K) = \mathcal{B}(2\mathbb{P}e|_K) + \mathbb{P}e|_K - 1$$

which, upon substitution into (4c), recovers the well known 1D Scharfetter-Gummel scheme originally also proposed as "exponential fitting" by Allen and Southwell in [2].

3.3.2. The 3D SG Artificial Diffusion Method. In a 3D framework a straightforward extension of the 1D Scharfetter-Gummel stabilization (4g)- (4h) can be obtained by introducing a 3×3 diagonal stabilizing tensor $\underline{\underline{\Phi}}^K$ defined on each element $K \in \mathcal{T}_h$ as follows

$$(4i) \quad \underline{\underline{\Phi}}_{ii}^K = \frac{\langle \Pi_1^K(e^{(\varphi_h - \varphi_M)/V_{th}}) \rangle_K \partial_{x_i} \varphi}{\partial_{x_i} \Pi_1^K(e^{(\varphi_h - \varphi_M)/V_{th}}) V_{th}} - 1 \quad i = 1, 2, 3.$$

where we have used, as a reference value for the potential reference to avoid overflow exceptions in the machine evaluation of (4i), the maximum φ_M of φ_h in K .

The 3D approximate electron current density is then

$$(4j) \quad \mathbf{J}_{n,K} = q\mu_n \langle n \rangle_K \mathbf{E}_K + qD_n (\underline{\underline{\mathcal{I}}} + \underline{\underline{\Phi}}_K) \nabla n_h$$

where $\underline{\underline{\mathcal{I}}}$ is the 3×3 identity tensor. In a completely similar manner we have the relation for hole current density

$$(4k) \quad \mathbf{J}_{p,K} = q\mu_p \langle p \rangle_K \mathbf{E}_K - qD_p (\underline{\underline{\mathcal{I}}} + \underline{\underline{\Phi}}_K) \nabla p_h$$

where

$$(4l) \quad \underline{\underline{\Phi}}_{ii}^K = \frac{\langle \Pi_1^K(e^{(\varphi_m - \varphi_h)/V_{th}}) \rangle_K \partial_{x_i} \varphi}{\partial_{x_i} \Pi_1^K(e^{(\varphi_m - \varphi_h)/V_{th}}) V_{th}} - 1 \quad i = 1, 2, 3,$$

φ_m being the minimum of φ over K . It is immediate to check that the two proposed novel approximations (4j) and (4k) satisfy all cases C1, C2 and C3 in Sect. 3.3.1.

4. NUMERICAL EXPERIMENTS

In order to compare the performance of the methods of Sect. 3 we use the FEMOS computational platform for the numerical simulation of three 3D devices: 1) a p - n diode; 2) a n -MOS device; and 3) a p -MOS device in on and off working conditions. While the diode and the n -MOS devices are coming out from ideal structures, the p -MOS is the result of a realistic 2D-process simulation accounting for non ideal doping profiles. This last test structure is a severe benchmark to highlight the accuracy and the stability of the different density current calculation methods.

4.1. Diode. The first structure is a semiconductor region with a p - n junction whose dimensions are $\Omega = (0, 0.3)^3 \mu m^3$. A Gaussian implantation of donors with a peak of $10^{19} [cm^{-3}]$ and a depth of $0.15 [\mu m]$ Fig.1b is made over an p -type region with a constant acceptor profile of $10^{18} [cm^{-3}]$ magnitude. Two contacts are defined for each of the doped regions: for the n -type part a rounded-shape contact is used (Top), while the p -type part is contacted at the bottom face (see Fig.1a) (Body). Contacts are considered as a pure Ohmic-type with appropriate Dirichlet boundary conditions: the Top is maintained at ground while the Body is ramped at $0.8[V]$. In Fig.2 the results of the calculation of the current density flux for electrons and holes in the semiconductor bulk are represented through streamlines connecting the Body with the Top contact. As expected the current calculation obtained with method DDFE (eq. (2)) is affected by a critical behavior, in particular close to and inside the n -junction as shown in Fig.2a and Fig.2b where instability has to be ascribed to numerical cancellation of the drift and diffusion contributions. Results get definitely better by employing method B using Eqns. (4j) and (4k) where the improvement can be appreciated in Fig.2e and Fig.2f. However, a careful inspection of the hole current density reveals that some numerical instability is still evident inside the n -junctions. The extension of the 1D SGscheme to 3D provided by method A in Eq.(3f) and (3k) results in the streamlines presented in Fig.2c and Fig.2d: no spurious instability can be observed anymore and our calculations are in excellent agreement with the results of a commercial code (not shown here).

4.2. p -MOS structure. The comparison of the different current computational methods has also been carried out on a p -channel MOSFET. The doping profiles have been obtained by using a 2-D process simulator with implantation and diffusion steps [1] with the purpose to have a realistic doping as reported in Fig.3a with a *GateLength* : $180nm$ and a *GateOx* : $4.5nm$. The presence of floating non-compensated p -type regions in the channel body increases the computational difficulties. The 2D doping profile has been then extruded in three spatial dimensions, and the generated mesh is shown in Fig.3b where the device contact has been highlighted with purple color (the body contact is not shown in the picture but is located in the down face of the silicon region). The Gate contact is then negatively

biased to build the standard $I_D - V_G$ with the drain bias kept at 0.1 V. The calculation of the current at the contacts is carried out by extending to the 3D case the approach proposed in [16] for the 2D case. The novel formulation, known as *residual method*, is based on the approach proposed in [17]. Computed currents are reported in Fig.4a (lines) and compared with the commercial tool results [1] (symbols). The two computed curves are virtually indistinguishable. Regarding the calculation of \mathbf{J}_p , the numerical difficulties found with Method DDFE are still confirmed as clearly depicted in Fig.4b not only inside the p -type region but also around the floating regions present in the body (the visualization are referred to the bias conditions $V_G = -1.0V$ and $V_D = -0.1V$). The marginality found using formula (4k) in Sect. 4.1 is increased as reported in Fig.4d: this comes by the fact that the evaluation of the coefficient in the formula (4i) is again undergoing numerical problems related to roundoff error. However Method B is giving a much better current density evaluation with respect to the pure application of the Drift-Diffusion approach at element wise level. We conclude this section by noting that, again, the best description of the expected physical behavior of the device is obtained by adopting Method A, that turns out to provide an accurate and stable 3D extension of the 1D SG formula, as clearly demonstrated by Fig.4c.

4.3. n -MOS structure with II. As a final simulation test we have adopted the n -channel MOSFET structure of Fig.5a (*GateLength* : 100nm; *GateOx* : 30nm and contacts $S = source, Gate, D = drain, Body$) with analytical doping profiles. Numerical validation of the on-state is reported in Fig.5b for different values of drain bias. Our results (continuous lines) are compared with those of a commercial tool [1] (symbols) obtaining a very good agreement: electron and hole mobilities are assumed to be constant $\mu_n = 1417, \mu_p = 470.5[cm^2V^{-1}s^{-1}]$. Fig.6 shows the results of the simulation in the case of reverse bias, where the II mechanism is activated as a generation term by employing Method A for the current calculation inside the Gummel map algorithm. The drain-to-bulk breakdown is found to occur at around $V_D = -1V$ and in the linear scale plot we have highlighted with the cross-symbol the reduction of the drain bias incremental step automatically determined due to high difficulty in convergence when the II generation rate significantly increases and dominates over the other R/G phenomena. Fig.7 visualizes the increase of the II generation term with the drain inverse voltage: breakdown is starting at the drain-channel junction under the gate and proceeds towards the bulk along the junction profile. Fig.8 reports the visualization of \mathbf{J}_n in both the off and on states of the device, calculated using Method A: as expected in the on-state the electron current density is confined under the gate from drain-to-source while in the off-state it is flowing from source-to-drain and from source-to-body in accordance to physical insight.

5. CONCLUSIONS

In this article we have addressed the problem of representing in 3D the carrier current density by extending the beneficial properties emanating from the classic 1D Scharfetter-Gummel difference formula. To this purpose, we have adopted the Galerkin Finite Element Method for the numerical simulation of the Drift-Diffusion model in the 3D case, and we have proposed two novel methods for current density evaluation, denoted method A and B, to which, for comparison, we have added

also the basic method DDFE using the DD formula. The three schemes compute a piecewise constant approximation of the current density over a tetrahedral partition of the device domain.

Method DDFE turns out to provide the worst results in the test experiments. Method B is a 3D extension of the method of optimal artificial diffusion and gives reasonably accurate results. Method A is a natural extension of the 1D SG approach based on a primal-mixed formulation endowed with a suitable quadrature formula for the approximate evaluation of the averaged electrical conductivity. It is by far the best of the three considered approaches, providing simulation results in excellent agreement with a commercial software. The three FE formulations are numerically verified in the study of realistic 3D structures, also including the presence of Impact Ionization phenomena. Even in this latter case, Method A is able to correctly describe the complex carrier flow patterns inside the device bulk and to track the I-V curve of the device up to the avalanche breakdown region.

Despite the proposed formulations are illustrated and validated in the study of the classic DD transport model in semiconductors, they can be applied in a straightforward manner to the numerical treatment of general conservation laws for advective-diffusive fluxes where the advective term is in gradient form, as is the case for ion electrodiffusion in electrochemistry and biology with the Poisson-Nernst-Planck model [25] and hydrodynamic and quantum-corrected charge transport in semiconductors [13, 12, 11].

REFERENCES

- [1] *Sentaurus Device User Guide*. Synopsis Inc., 2013.
- [2] D. N. G. Allen and R. V. Southwell. Relaxation methods applied to determine the motion, in two dimensions, of a viscous fluid past a fixed cylinder. *Quart. J. Mech. Appl. Math.*, 8:129–145, 1955.
- [3] R. E. Bank, J. F. Burgler, W. Fichtner, and R. K. Smith. Some upwinding techniques for finite element approximations of convection-diffusion equations. *Numer. Math.*, 58:185–202, 1990.
- [4] R.E. Bank, D. Rose, and W. Fichtner. Numerical methods for semiconductor device simulation. *SIAM Journal on Scientific and Statistical Computing*, 4(3):416–435, 1983.
- [5] R.E. Bank, D. Rose, and W. Fichtner. Numerical methods for semiconductor device simulation. *Electron Devices, IEEE Transactions on*, 30(9):1031–1041, 1983.
- [6] F. Brezzi, L. Marini, and P. Pietra. Numerical simulation of semiconductor devices. *Comp. Meths. Appl. Mech. Engrg*, 75:493–514, 1989.
- [7] F. Brezzi, L. Marini, and P. Pietra. Two-dimensional exponential fitting and applications to drift-diffusion models. *SIAM Journal on Numerical Analysis*, 26(6):1342–1355, 1989.
- [8] F. Brezzi, L.D. Marini, P.A. Markowich, and P. Pietra. On some numerical problems in semiconductor device simulation. In G. Toscani, V. Boffi, and S. Rionero, editors, *Mathematical Aspects of Fluid and Plasma Dynamics*, volume 1460 of *Lecture Notes in Mathematics*, pages 31–42, 1991.
- [9] A. N. Brooks and T. J.R. Hughes. Streamline Upwind/Petrov-Galerkin formulations for convection dominated flows with particular emphasis on the incompressible Navier-Stokes equations. *Computer Methods in Applied Mechanics and Engineering*, 32(120133):199 – 259, 1982.
- [10] P. Cogež, M. Graef, B. Huizing, R. Mahnkopf, H. Ishiuchi, N. Ikumi, S. Choi, J. H. Choi, C. H. Diaz, Y. C. See, P. Gargini, T. Kingscott, and I. Steff. The International Technology Roadmap for Semiconductors: 2013. Technical report, Jointly sponsored by ESIA, JEITA, KSIA, TSIA and SIA, 2013.
- [11] C. de Falco, J. W. Jerome, and R. Sacco. Quantum-corrected drift-diffusion models: Solution fixed point map and finite element approximation. *Journal of Computational Physics*, 228(5):1770 – 1789, 2009.

- [12] C. de Falco, A. L. Lacaita, E. Gatti, and R. Sacco. Quantum-corrected drift-diffusion models for transport in semiconductor devices. *J. Comp. Phys.*, 204:533–561, 2005.
- [13] A. Forghieri, R. Guerrieri, P. Ciampolini, A. Gnudi, M. Rudan, and G. Baccarani. A new discretization strategy of the semiconductor equations comprising momentum and energy balance. *Computer-Aided Design of Integrated Circuits and Systems, IEEE Transactions on*, 7(2):231–242, Feb 1988.
- [14] H. K. Gummel. A self-consistent iterative scheme for one-dimensional steady state transistor calculations. *IEEE Trans. Electron Devices*, pages 455–465, 1964.
- [15] H. K. Gummel and D. Scharfetter. Large-signal analysis of a silicon read diode oscillator. *IEEE Trans. Electron Devices*, pages 64–77, 1969.
- [16] R. Gusmeroli and A. S. Spinelli. Accurate boundary integrals calculation in semiconductor device simulation. *IEEE Trans. Electron Devices*, 53:1730–1733, 2006.
- [17] T.J.R. Hughes, G. Engel, L. Mazzei, and M.G. Larson. The continuous Galerkin method is locally conservative. *Journal of Computational Physics*, 163:467–488, 2000.
- [18] J. W. Jerome. *Analysis of Charge Transport*. Springer, 1996.
- [19] P.A. Markowich. *The Stationary Semiconductor Device Equations*. Computational Microelectronics. Springer-Verlag, 1986.
- [20] A. Mauri, R. Sacco, and M. Verri. Electro-thermo-chemical computational models for 3D heterogeneous semiconductor device simulation. arXiv:1307.3096, to appear in Applied Mathematical Modeling.
- [21] S. Micheletti, A. Quarteroni, and R. Sacco. Current-voltage characteristics simulation of semiconductor devices using domain decomposition. *Journal of Computational Physics*, 119(1):46–61, 1995.
- [22] G. Novielli, A. Ghetti, E. Varesi, A. Mauri, and R. Sacco. Atomic migration in phase change materials. In *Electron Devices Meeting (IEDM), 2013 IEEE International*, pages 22.3.1–22.3.4, Dec 2013.
- [23] A. Quarteroni and A. Valli. *Numerical Approximation of Partial Differential Equations*. Springer, 2008.
- [24] J. Roberts and J. M. Thomas. Mixed and hybrid methods. *Handbook of Numerical Analysis*, 2:523–633, 1991.
- [25] I. Rubinstein. *Electrodiffusion of Ions*. SIAM, 1990.
- [26] R. Sacco, L. Carichino, C. de Falco, M. Verri, F. Agostini, and T. Gradingner. A multiscale thermo-fluid computational model for a two-phase cooling system. *Computer Methods in Applied Mechanics and Engineering*, 282(0):239 – 268, 2014.
- [27] S. Selberherr. *Analysis and Simulation of Semiconductor Devices*. Springer-Verlag, Wien, 1984.
- [28] J. Xu and L. Zikatanov. A monotone finite element scheme for convection-diffusion equations. *Mathematics of Computation*, 68:1429–1446, 1999.
- [29] L. T. Zikatanov and R. D. Lazarov. An exponential fitting scheme for general convection-diffusion equations on tetrahedral meshes. *Computational and Applied Mathematics*, 1:60–69, 2012.

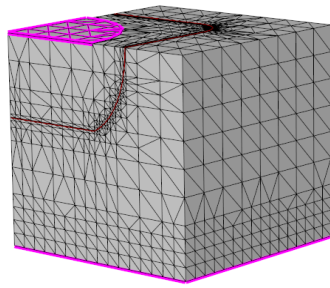
¹ MODELING AND SIMULATIONS GROUP MICRON TECHNOLOGY VIA OLIVETTI 2, AGRATE BRIANZA, ITALY, ² IBM ITALIA, VIA CIRCONVALLAZIONE IDROSCALO, 20090, SEGRATE (MI), ITALY, ³ STMICROELETRONICS, VIA OLIVETTI 2, 20864, AGRATE BRIANZA (MB), ITALY, ⁴ DIPARTIMENTO DI MATEMATICA, POLITECNICO DI MILANO PIAZZA L. DA VINCI 32, 20133 MILANO, ITALY

E-mail address: aureliogianc@micron.com

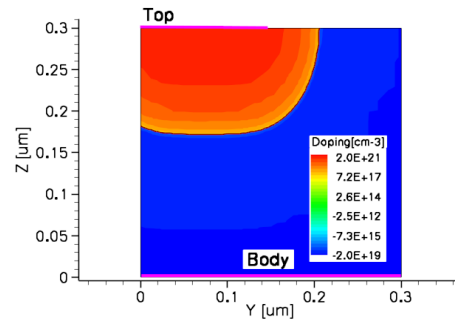
E-mail address: andrea.bortolossi@it.ibm.com

E-mail address: giovanni.novielli@st.com

E-mail address: riccardo.sacco@polimi.it



(A) Mesh



(B) 2D cut of Mesh for doping profile visualization

FIGURE 1. Diode structure: Left: doping. Right: mesh.

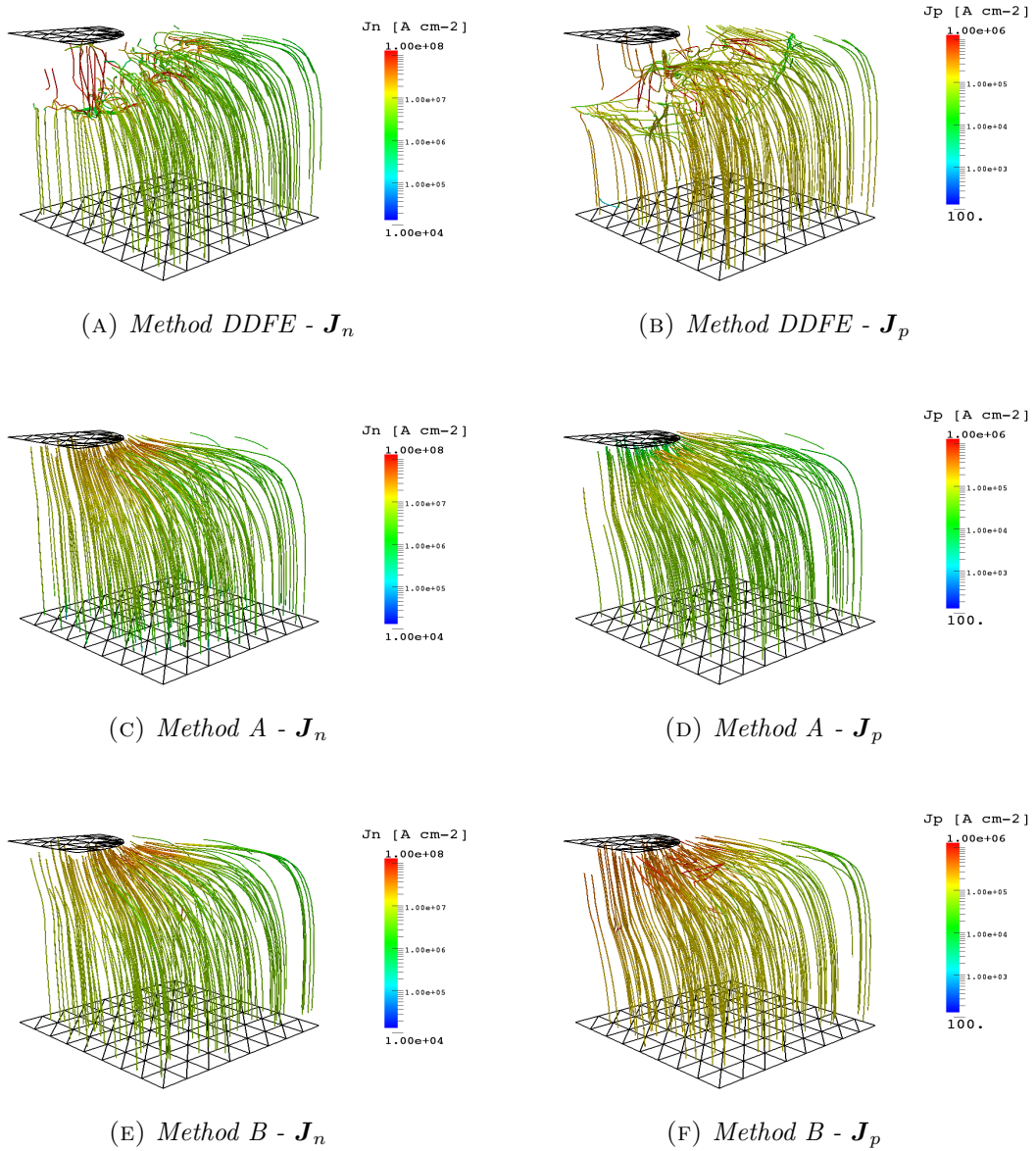


FIGURE 2. Electron (left column) and hole (right column) current densities of Diode test case at $V_{body} = 0.8[V]$. Top: Method DDFE. Middle: Method A. Bottom: Method B.

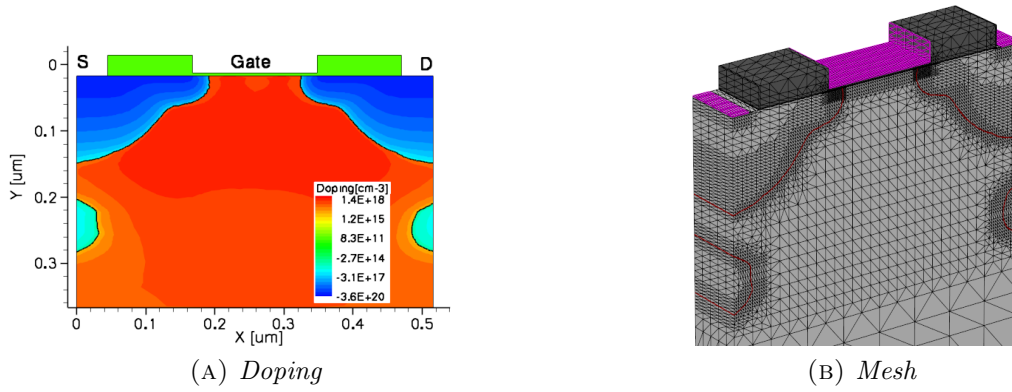


FIGURE 3. *p*-MOSFET structure: Left: Doping. Right: Mesh.

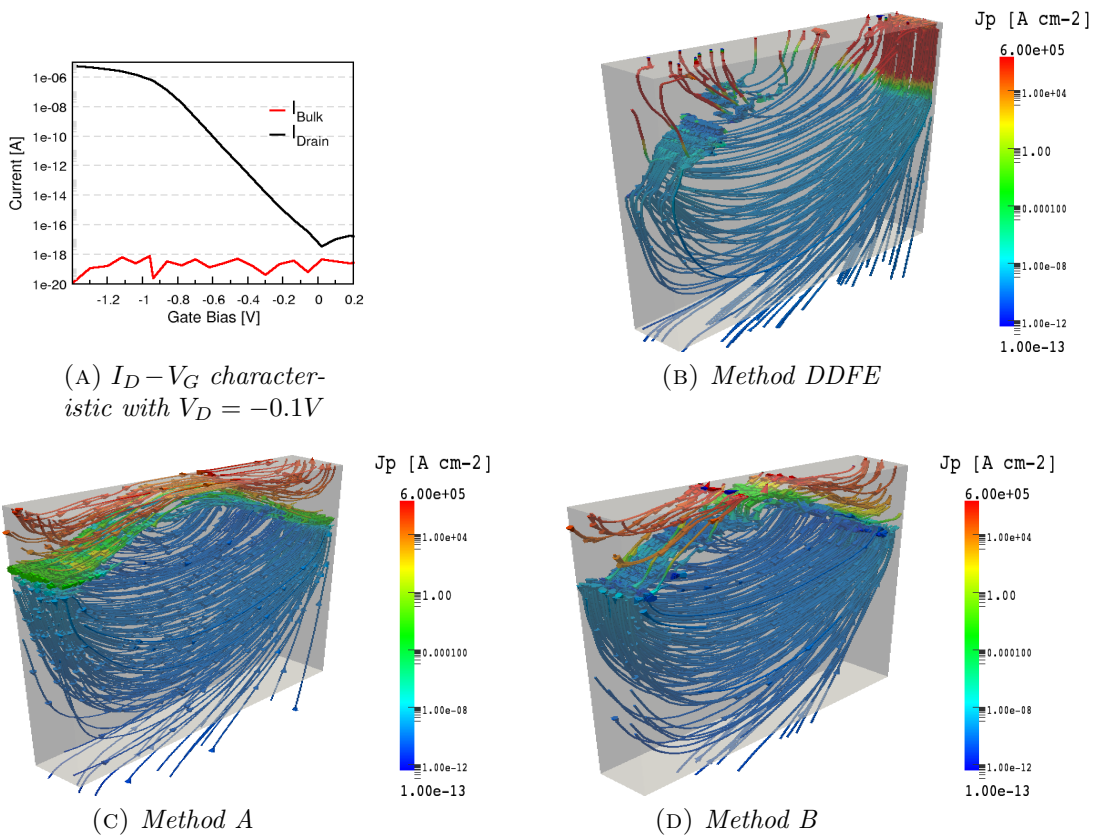
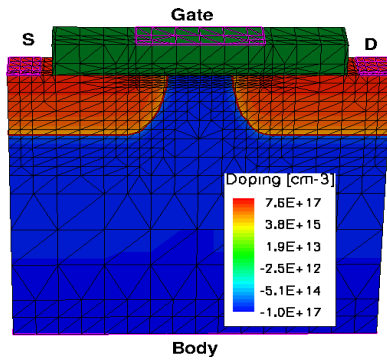


FIGURE 4. $I_D - V_G$ and hole current density calculation of *p*-MOSFET at $V_G = -1.0V$ and $V_D = -0.1V$: Top left: $I_D - V_G$. Top right: Method DDFE. Bottom left: Method A. Bottom right: Method B.



(A) Mesh and Doping

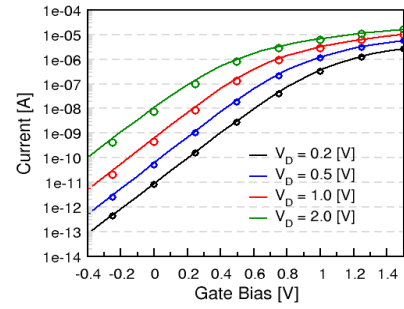
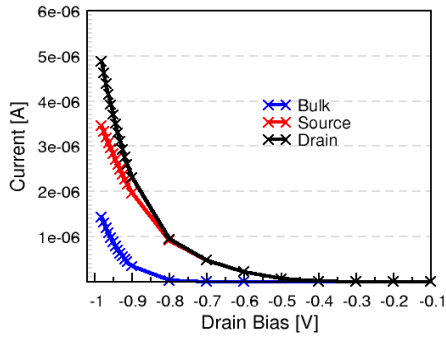
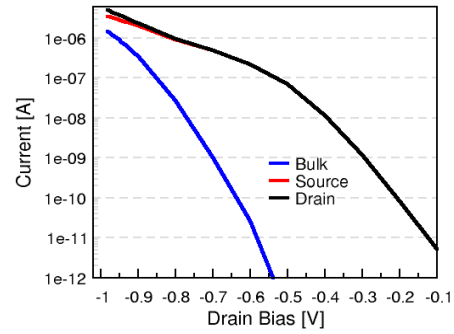
(B) $I_D - V_G$ characteristics

FIGURE 5. n -MOS structure and numerical validation in on-state: Left: Doping and Mesh. Right: $I_D - V_G$.



(A) linear scale



(B) log-scale

FIGURE 6. n -MOSFET: off-state characteristic. Left: linear scale. Right: log-scale.

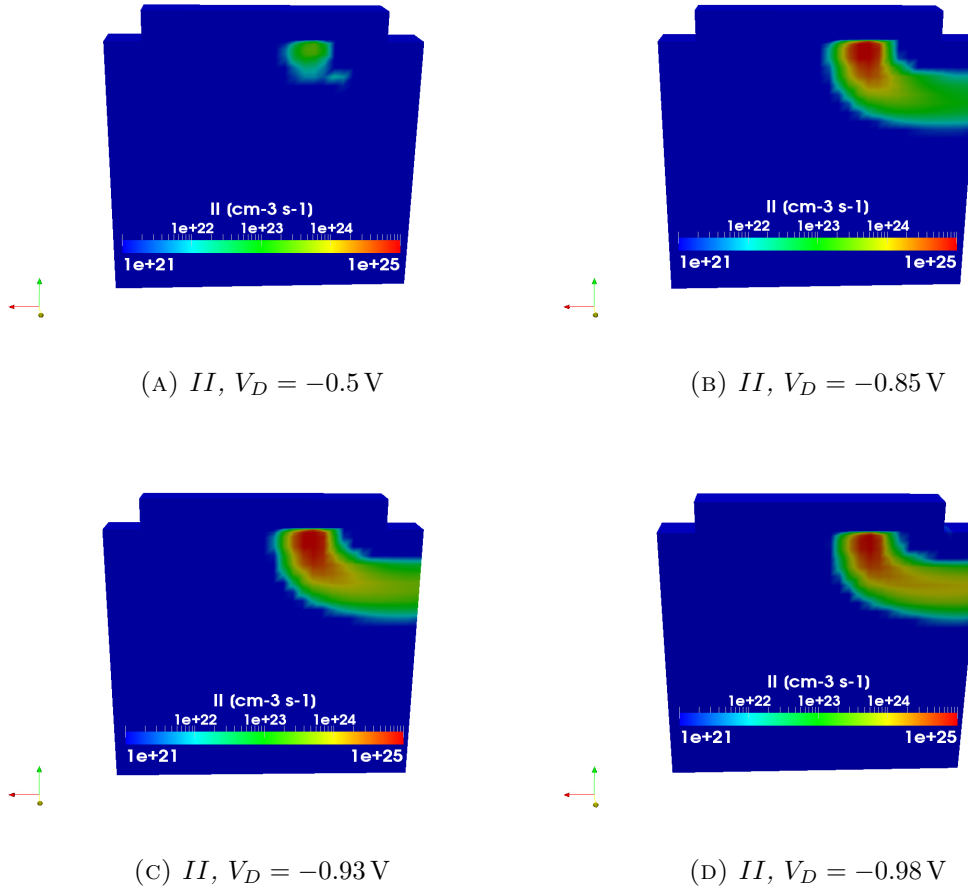


FIGURE 7. n-MOSFET: II generation term. Top left: $V_D = -0.5$ V. Top right: $V_D = -0.85$ V. Bottom left: $V_D = -0.93$ V. Bottom right: $V_D = -0.98$ V.

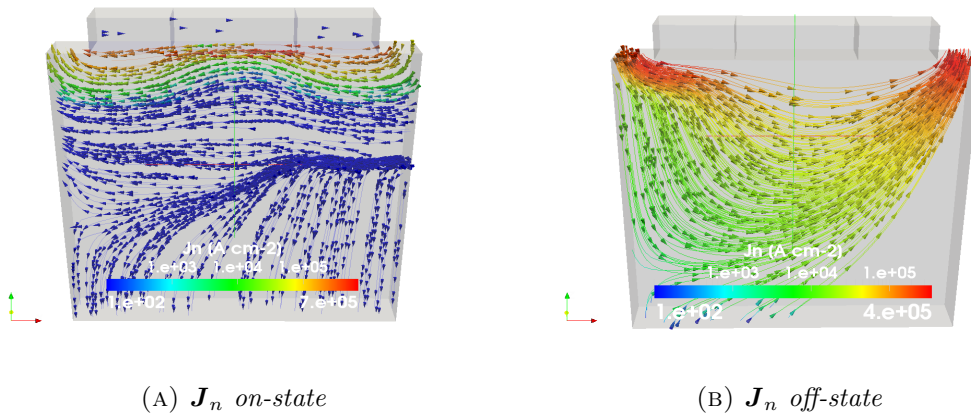


FIGURE 8. n-MOSFET: electron current density streamlines obtained with method A. Left: on-state. Right: off-state.